One of the important properties of nanotubes is their ability to withstand extreme strain in tension (up to 40 per cent). The tubes can recover from severe structural distortions. The resilience of a graphite sheet is manifested in this property, which is due to the ability of carbon atoms to rehybridize. Any distortion of a tube will change the bonding of the nearby carbon atoms and in order to come back to the planar structure, the atoms have to reverse to sp^2 hybridization. If the tube is subjected to elastic stretching beyond a limit, some bonds are broken. The defect is then redistributed along the tube surface.

4.8 Physical Properties

Nanotubes have a high strength-to-weight ratio (density of 1.8 g/cm^3 for MWNTs and 0.8 g/cm^3 for SWNTs). This is indeed useful for lightweight applications. This value is about 100 times that of steel and over twice that of conventional carbon fibres. Nanotubes are highly resistant to chemical attack. It is difficult to oxidize them and the onset of oxidation in nanotubes is 100 °C higher than that of carbon fibres. As a result, temperature is not a limitation in practical applications of nanotubes.

The surface area of nanotubes is of the order of 10–20 m^2/g, which is higher than that of graphite but lower than that of mesoporous carbon used as catalytic supports where the value is of the order of 1000 m^2/g.

Nanotubes are expected to have a high thermal conductivity and the value increases with decrease in diameter (Ref. 20). The thermal conductivity of single nanotubes were shown to be comparable to diamond and in-plane graphite (Ref. 21).

4.9 Applications

The use of nanotubes as electrical conductors is an exciting possibility. A nanotube-based single molecule field effect transistor has already been built (Ref. 22). The performance of this device is comparable to that of semiconductor-based devices, but the integration of this into circuits will require a lot of effort. One of the problems associated with such devices is the need to make contacts and adopt newer kinds of approaches. It has been seen that it is possible to fabricate-nanotube-based connectors. Such interconnectors between structures patterned on substrates have also been made (Ref. 23).

It is possible to construct a heterojunction by having a junction between nanotubes of different helicities. This approach facilitates the creation of a device with one molecule. An approach for making devices of this kind has been developed in Bangalore. The pyrolysis of a mixture of metallocenes with thiophene yields excellent quality junction nanotubes (Ref. 24). Various metallocenes such as ferrocene, cobaltocene and nickelocene have also been tried. The interesting aspect is that the three arms of the *Y* junction can have different helicities thus yielding a molecular transistor. Although plenty of '*y*' type junctions are synthesized, the transistor action was demonstrated only recently (Ref. 25).

One of the areas of immediate commercial application of nanotubes is CNT-based field emission displays. Here CNTs act as electron emitters at lower turn on voltages and high emissivity. The turn on voltage on a practical device developed by Samsung is 1 V/micrometer and the brightness measured is of the order of 1800 candela/m^2 at 4 V/micrometer (Ref. 26). With the addressing of individual pixels, the method will soon be ready for commercial exploitation. An image of a running video on a 5-inch diagonal display is shown in Fig. 4.6 (Plate 4). The emission is due to patterned SWNTs. One of the things needed in the process of commercial application is the capability to make aligned CNTs on substrates, which is possible with CVD-based methods. Field emission is stable in air, and electron emission is stable for several hours. Therefore, there is no practical limitation in CNTs for this application.

Nanotube tips can be used as nanoprobes. The possibility using AFM and STM tips has also been demonstrated. The functionalization of tips can be used in chemical force microscopy wherein a chemical functionality interacts with an appropriate one on the substrate. Such studies help one deduce information such as the strength of a chemical bond. Being flexible, the probes are not susceptible to frequent crashes, unlike in the case of normal STM tips. The tubes can also penetrate into crevices, which facilitates sub-surface imaging.

Research is also being carried out to assess the ability of carbon nanotubes to store hydrogen (Ref. 27). The storage occurs both in between and inside the nanotube bundles. Research has shown that the amount of hydrogen stored is comparable to that in the best storage materials such as metal hydrides. The application of this kind of storage will be important for fuel cell applications for automobiles where the storage of hydrogen is one of the critical factors. However, in order to make this feasible, it is important to store hydrogen to the extent of 5 per cent of the nanotube mass. Achieving this quantity appears to be a problem, though the intake and release are feasible.

A flow sensor using nanotubes has also been demonstrated (Ref. 28). In this device, liquids flow through aligned single-walled nanotubes supported on a substrate. The flow generates an electrical potential of the order of a few millivolts. The potential is sensitive both to the flow velocity as well as the dipole moment of the analyte. Gas flow sensors have also been developed along similar lines. Nanotube-based gas sensors have also been developed which utilize the narrow channels of the tubes that are of a comparable dimension to molecules (Ref. 29). Nanotube-based filters have also been demonstrated (Ref. 30). Here a liquid containing a mixture of molecules such as petroleum is separated into the components by filtration. Such an approach makes it possible to filter out bacteria, viruses and chemicals from water. The most important aspect in the development of such a filter is the fabrication of a mechanically stable filter with aligned carbon nanotubes.

4.10 Nanotubes of Other Materials

In principle, any planar structure should be able to curl and make a tubular structure. Certain clays such as christolite and imogolite are found in tubular form. The structural characteristics of CNTs such as helicity and rotational disorder, are found in these clays too. The first nanotube structure found with inorganics has been reported with WS_2 and MoS_2. These structures consist of alternating layers of W/Mo and S. They

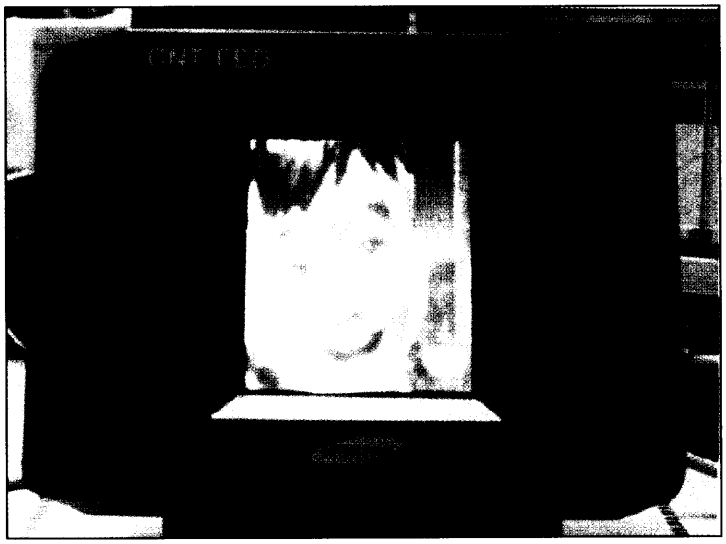

Fig. 4.6: *Picture of a 5" diagonal active display developed by Samsung Corporation. Reused with permission from Chung, et al. (Ref. 25). Copyright 2002, American Institute of Physics.*

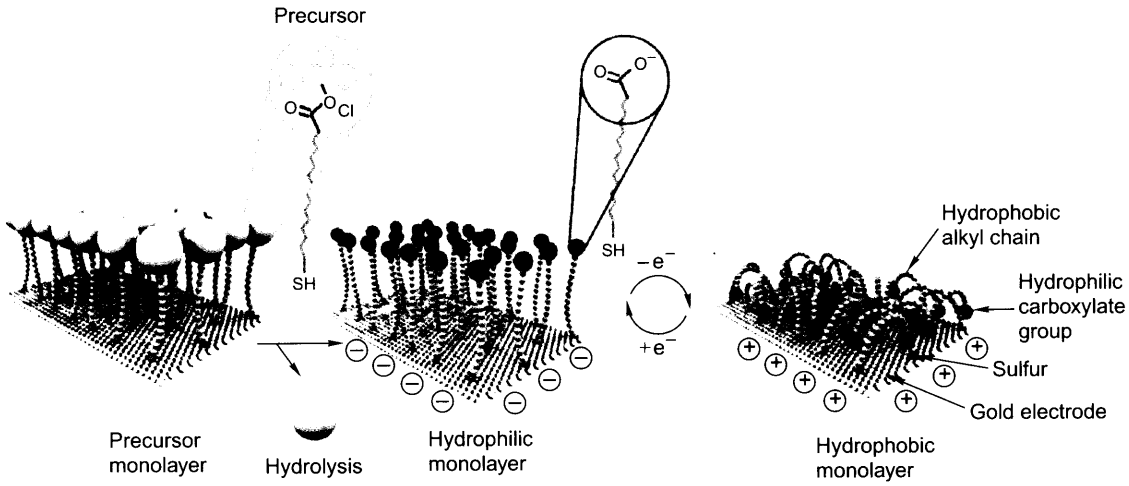

Fig. 5.19: *Schematic showing a monolayer which changes conformation with applied electric field. As a result of this, the polarity of the surface can be switched reversibly by changing the electric field. This allows one to control the wetting behavior of metal plates. Reprinted with permission from Lehann, et al. (Ref. 32). Copyright (2003) AAAS.*

have an excellent lubricating property, and they roll on the substrate. Nanotubes have been made with BN and BCN as well as with $B_xC_yN_z$.

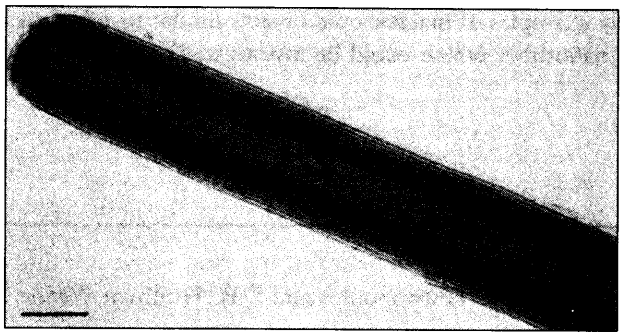

Fig. 4.7: *Electron micrograph of part of a WS_2 based nanotube (Ref. 30). The tube is assumed to be hollow. The contrast within the tube is attributed to the outer wall, perpendicular to the tube. The scale bar is 10 nm. Copyright Nature. Used with permission from the author.*

A variety of polyhedral and tubular structures of WS_2 have been obtained by heating a thin tungsten film in H_2S (Ref. 31). The tubes observed are hollow and are closed at ends. An image of a tube is shown in Fig. 4.7. The curling of a graphite-like sheet of WS_2 leads to the creation of defects. Such defects can be nucleated by high temperature treatment. Structures other than tubes, such as onions, have also been made in this way. These are, in general, called inorganic fullerenes. The properties of inorganic fullerenes and inorganic nanotubes have been thoroughly researched. Analogous to carbon nanotubes, several properties of these systems have also been studied.

Review Questions

1. How would one classify carbon nanotubes? What are the various kinds of carbon nanotubes?
2. How would one get the (n,m) indices from the diameter?
3. What are the diameter-dependent properties of nanotubes?
4. Why is it not possible to inset an arbitrary tube into a given tube?
5. What are the other materials which can form nanotubes?
6. Are there specific properties of nanotubes which will be different in multiwalled and single-walled nanotubes?
7. What are the unique properties of nanotubes and how would one study those?

8. Can one extend the knowledge of the chemistry of fullerenes into carbon nanotubes? What are such properties?
9. How can be the properties of 'tubes' of cylinders used in the case of nanotubes?
10. From the everyday examples of macroscopic objects similar to tubes, such as iron pipes, suggest a few properties of nanotubes which could be investigated.

References

1. Kratschmer, W., L.D. Lamb, K. Fostiropoulos and D.R. Huffman, *Nature*, **347**, **354** (1990).
2. Iijima, S., *Nature*, **354** (1991), p. 56.
3. Ajayan, P.M. and T.W. Ebessen, *Rep. Prog. Phys.*, **60** (1997), p. 1025.
4. Guo, T., P. Nikolaev, A. Thess, D.T. Colbert and R.E. Smalley, *Chem. Phys. Lett.*, **243** (1995), p. 49.
5. Amelinckx, S., X.B. Zhang, D. Bernaerts, X.F. Zhang, V. Ivanov and J.B. Nagy, *Science*, **265** (1994), p. 635.
6. Tsang, S.C., P.J.F. Haris and M.L.H. Green, *Nature*, **362** (1993), p. 520.
7. Rao, C.N.R., R. Sen, B.C. Satishkumar and A. Govindaraj, *Chem. Commun.*, (1998), p. 1525.
8. Chen, Y.K., A. Chu, J. Cook, M.L.H. Green, P.J.F. Haris, R. Heesom, M. Humphries, J. Sloan, S.C. Tsang and J.C.F. Turner, *J. Mat. Chem.*, **7** (1997), p. 545.
9. Serpahin, S., D. Zhou, J. Jiao, J.C. Withers and R. Roufty, *Nature*, **362** (1993), p. 503.
10. Gundiah, G., G.V. Madhav, A. Govindaraj and C.N.R. Rao, *J. Mater. Chem.*, **12** (2002), p. 1606.
11. Helveg, S., C. Lopes–Cartes, J. Sehested, P.L. Hansen, B.S. Clausen, J.R. Rostrup–Nielsen, F. Abid-Pedersen and J.K. Norskov, *Nature*, **427** (2004), p. 426.
12. Satishkumar, B.C., P.J. Thomas, A. Govindaraj and C.N.R. Rao, *Appl. Phys. Lett.*, **77** (2000), p. 2530.
13. Ajayan, P.M. in *Nanostructured Materials and Nanotechnology*, (2002), Hari Singh Nalwa, (ed.) Academic Press, San Diego.
14. Bursill, L.A., P.A. Stadelmann, J.L. Peng and S. Prawer, *Phys. Rev. B.*, **49** (1994), p. 2882.
15. Hiura, H., T.W. Ebessen, K. Tanigaki and H. Takahashi, *Chem. Phys. Lett.*, **202** (1993), p. 509.
16. Maeda, Y., S. Kimnra, M. Kanda, Y. Harashima, *et al.*, *J. Am. Chem. Soc.*, **127** (2005), p. 10287.
17. Dresselhaus, M.S., G. Dresselhaus and P.C. Eklund, (1996), *Science of Fullerenes and Carbon Nanotubes*, Academic Press, New York.
18. Langer, L., V. Bayot, E. Grivei, J.P. Issi, J.P. Heremans, C.H. Olk, L. Stockman, C. Van Haesendonck and Y. Bruynseraede, *Phys. Rev. Lett.*, **76** (1996), p. 479.
19. Treacy, M.M.J., T.W. Ebessen and J.M. Gibson, *Nature*, **381** (1996), p. 678.

20. Fuji, M., X. Zhang, H.Q. Zie, H. Ago, K. Takashashi, T. Iknta, H. Abe and T. Shimizn, *Phys. Rev. Lett.*, **95** (2005) p. 65502.
21. Hone, J., M. Whitney, C. Piskoti and A. Zettel, *Phys. Rev.*, **59** (1999), p. R2514.
22. Tans, S.J., A.R.M. Verschueren and C. Dekker, *Nature*, **393** (1998), p. 49.
23. Homma, Y., Y. Kobayashi, T. Ogino and T. Yamashita, *Appl. Phys. Lett.*, **81** (2002), p. 2261.
24. Satishkumar, B.C., P.J. Thomas, A. Govindaraj and C.N.R. Rao, *Appl. Phys. Lett.*, **77** (2000), p. 2530.
25. Bandaru, P.R., C. Dario, S. Jin, and A.M. Rao, *Nature Materials*, **4** (2005) p. 663.
26. Chung, D.S., S.H. Park, H.W. Lee, J.H. Choi, S.N. Cha, J.W. Kim, J.E. Jang, K.W. Min, S.H. Cho, M.J. Yoon, J.S. Lee, C.K. Lee, J.H. Yoo, J.M. Kim, J.E. Jung, Y.W. Jin, Y.J. Park and J.B. You, *Appl. Phys. Lett.*, **80** (2002), p. 4045.
27. Dillon, A.C., K.M. Jones, T.A. Bakkedahl, C.H. Kiang, D.S. Bethune and M.J. Heben, *Nature*, **386** (1997), p. 377.
28. Ghosh, S., A.K. Sood, and N. Kumar, *Science*, **299** (2003), p. 1042.
29. Modi, A., N. Koratkar, E. Lass, B. Wei, and P.M. Ajayan *Nature*, **424** (2003) p.171.
30. Srivastava, A., O.N. Srivastava, S. Talapatra, R. Vajtai and P.M. Ajayan, *Nature Materials*, **3** (2004), p. 610.
31. Tenne, R., L. Margulis, M. Genut and G. Hodes, *Nature*, **360** (1992), p. 444.

Additional Reading

1. Rao, C.N.R. and A. Govindaraj, *Acc. Chem. Res.*, **35**, (2002), pp. 998–1007. (Carbon nanotubes)
2. Rao, C.N.R. and Minakshi Nath, *Dalton Trans.* (2003), pp. 1–24. (Inorganic nanotubes)
3. Dai, L. (ed.) (2006) *Carbon Nanotechnology: Recent Developments in Chemistry, Physics, Materials Science and Device Applications*, Elsevier.
4. Rao, C.N.R. and A. Govindaraj, (2005) *Nanotubes and Nanowires*, Royal Society of Chemistry.
5. Rao, C.N.R., A. Muller and A.K. Cheetham (eds) (2004), *The Chemistry of Nanomaterials: Synthesis, Properties and Applications*, Wiley–VCH, Weinheim.

Chapter 5

Self-assembled Monolayers

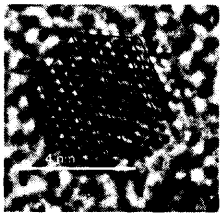

Self-assembled monolayers are important nanostructured systems which are two-dimensional nano assemblies. The structure of this assembly is such that it facilitates precise control of molecules. Various spectroscopic, scattering and imaging techniques have been used to understand the structure of self-assembled monolayers in detail. These assemblies have been used in a number of applications, mostly in the area of sensors. A protoptypical molecular nanomachine has been by built by using SAMs. The diversity of SAMs allows almost anything to be grown on them through appropriate chemistry.

Learning Objectives

- What are the various kinds of monolayers?
- What are self-assembled monolayers? What are their properties?
- What are their applications?
- How can one use them for nanotechnology?

5.1 Introduction

The bottom-up approach of manufacturing nano devices has been demonstrated very well. The most celebrated example is the iron corrals and the molecular abacus made by IBM researchers (Ref. 1). However, the use of such an approach to make devices, i.e. placing atoms one at a time to form a functional structure, cannot have a high throughput. The alternate approaches for making functional nanostructures must involve self-assembly. In this approach, once the process begins, structures are formed without external intervention. The structure organizes itself, on the basis of external conditions. The information required to form the structure is contained in the molecules themselves. The structure is organized by utilizing weak interactions such as hydrogen bonding, and van der Waals interactions, and there are numerous interactions of this kind in a structure which makes it stable. These are the interactions which make and sustain life, and there are numerous examples of such interactions in the world around us.

Monolayers are single-molecule thin layers prepared on surfaces. They can be assumed to be molecularly thin sheets of infinite dimension, just like ultra thin foils. They are among the simplest chemical systems

on which nanotechnological approaches can be practised. This feasibility of using monolayers arises from the simplicity of their design and molecular structure and from the user's ability to manipulate them at ease. The possibility of bringing about patterns of nanometer spatial resolution allows one to incorporate multiple functions within a small area.

The concept of monolayers was first introduced by Irving Langmuir in 1917, during his study of amphiphiles in water (Ref. 2). While spreading the amphiphiles on water, he found that the film formed had the thickness of one molecule. Later Katherine Blodgett was able to transfer the monolayer onto a solid support (Ref. 3). The spontaneous formation of a monolayer was first reported by Zisman, *et al.* in 1946 (Ref. 4). They observed the spontaneous monolayer formation of alkyl amines on a platinum surface. The field observed a tremendous growth when in 1983 Nuzzo and Allara found that ordered monolayer of thiols can be prepared on a gold surface by the adsorption of di-*n*-alkyl disulfides from dilute solutions (Ref. 5).

The name self-assembled monolayers (SAMs) indicates that their formation does not require the application of external pressure. The study of SAMs generates both fundamental as well as technological interest. Nature uses the same process of self-assembly to produce complex architectures. One such example is the formation of the cell membrane from lipid molecules through self-assembly. SAMs are ideal systems which can answer fundamental questions related to interfacial properties like friction, adhesion and wetting. They have been used to alter the wetting behavior of the condenser plates in steam engines. This is because the drop-wise condensation of steam enhances the efficiency of the engine as compared to the film-like condensation. In the latter case, the film acts as an insulator between the metal plate and steam. The two approaches used to make a monolayer of a molecule on a metal surface are discussed as follows.

1. The Langmuir—Blodgett Technique The Langmuir film is prepared by spreading amphiphilic molecules on a liquid surface. Considerable order can be achieved in these films by applying pressure. The film is then transferred to a solid substrate. The various steps involved during the preparation of Langmuir–Blodgett (L–B) films are shown in Fig. 5.1.

2. Self-assembly As mentioned earlier, the formation of a self-assembled monolayer does not require the help of an external driving force. Such a monolayer is formed when the metal (or any other substrate) surface is exposed to a solution containing the surfactant (Fig. 5.2).

5.2 Monolayers on Gold

Alkanethiolate monolayers (Ref. 6) grown on coinage metals (Au, Ag, Pt)—the molecular sheet is made of thiolate species (with long alkyl chains) and the substrate is one of the above metals—are structurally simple and easy to construct, which is why a larger number of studies have been conducted on them. It is important to mention that there are several other kinds of monolayers and a review of these is available in (Ref. 7).

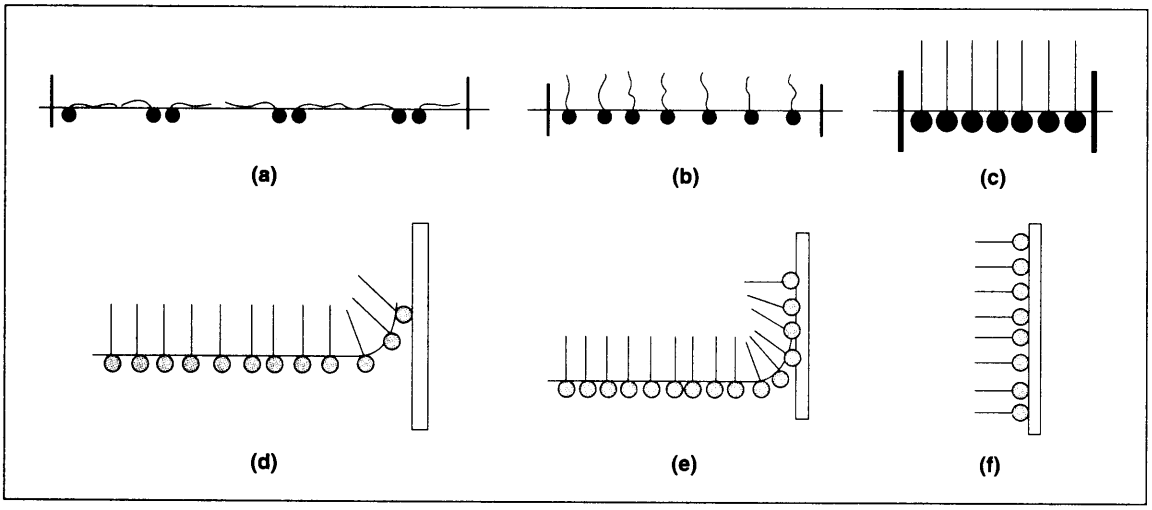

Fig. 5.1: *Langmuir–Blodgett methodology. (a) Surfactant in water. The black dot represents the head and the line represents the tail. The molecules are disordered. (b) Partially compressed monolayer by the pushing of a barrier across the film surface. (c) Ordered monolayer by the application of pressure. (d) Immersion of the substrate in an ordered film. (e) Transfer of the monolayer onto the substrate. (f) Densely packed monolayer on the substrate.*

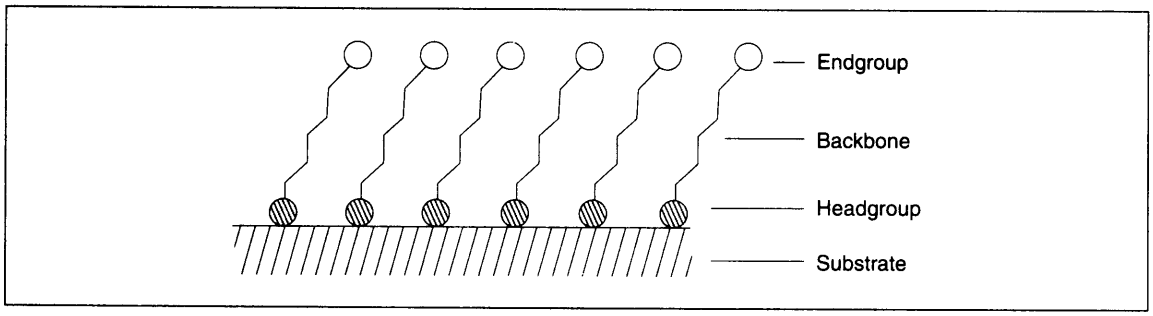

Fig. 5.2: *Schematic showing the basic structure of 2D SAMs.*

Gold has been the preferred substrate for a number of reasons. It is easy to make a thin gold film by thermal evaporation, and almost all kinds of supports can be used for film growth in the case of gold. For gold, there is no stable oxide at room temperature, though Au_2O_3 can be made by ozone exposure to Au films at room temperature. None of the commonly present gases of the atmosphere undergoes chemisorption on gold surfaces. Repeated solvent washes are adequate to make a gold surface atomically clean in most cases. The removal of carbonaceous deposits on gold can also be done by oxidizing them with a 'piranha' solution. This is a 1:3 mixture of 30 per cent H_2O_2 and concentrated H_2SO_4 at 100 °C. The solution is, however, highly reactive and should be handled cautiously. It is known to be an explosive mixture when kept in closed containers. Another way of cleaning a gold surface is by repeated cycling between

–0.3 and +1.5 V versus Ag/AgCl in a voltammetric cell. During the positive potential sweep, the surface is oxidized and in the negative sweep, the oxide is reductively removed. Cyclic voltammetric measurements carried out in this way facilitate the calculation of the effective surface area from the peak area.

5.2.1 Preparation

SAMs are prepared by dipping substrates such as evaporated gold films into a millimolar solution of the surfactant. The gold films of 500–2000 Å thickness are made on substrates. The solution is normally made in hexane for long-chain surfactants and in ethanol for short chain surfactants. The process of assembly of monolayers on the surface involves two stages. During the first stage, the surfactants are rapidly pinned on the surface, followed by a slow reorganization step, during the second stage, extending over several hours (Ref. 8). The exact kinetics of both these steps depend on parameters such as the concentration of the solution, length of the alkyl chain, etc. It is a standard practice to leave the substrate in the solution, face up ('face' refers to the gold coating), for periods ranging from 12–24 hours for complete self-assembly. Before being used, the monolayer surfaces are washed and blown dry with nitrogen. The kinetics of initial pinning can be monitored by a quartz crystal microbalance whereas the extent of organization can be studied through infrared spectroscopy. A monolayer of a mixture of alkane thiols can be prepared starting with a mixed solution of the concerned thiols. A mixed thiol monolayer can also be formed through a ligand place exchange reaction in which one surfactant molecule replaces another that is already present on the surface. Monolayers can be formed by microcontact printing wherein the thiol solution is used as ink on a stamp that is prepared from a polymer. This approach is especially useful in preparing patterned surfaces (see Section 5.5). Other methods that have been used to make SAMs include vapour phase deposition on molecules, LB methodology and potential-assisted deposition.

5.2.2 Structure

Two types of sites are available for the thiol chemisorption on the Au(111) surface, the on-top site and the hollow site. *Ab-Initio* calculations have shown that the charge of sulphur at the hollow site is –0.7e and that at the on-top site is –0.4e. Hence the hollow site is the energetically favorable one from the point of view of charge-transfer. Thiolate can migrate between the two adjacent hollow sites. This can happen either through the on-top site or through the bridge site. In both cases, the excited state will be polar. The excited state during such migration will then be stabilized by polar solvents. This is confirmed by the fact that ordered SAMs are formed in ethanol. Figure 5.3 shows the overlayer structure of the monolayer with sulphur atoms occupying alternative hollow sites above the Au(111) layer, giving a hexagonal $(\sqrt{3} \times \sqrt{3})$ $R30°$ unit cell (the symbolism refers to the crystallographic structure of an overlayer).

In this assembly, alkyl chains are in close contact with each other and the chains are fully stretched to form a zig-zag assembly. As a result of this close contact and due to the large distance between the sulphur atoms, the chains tilt. The tilt angle is 34° in the case of Au(111), but it is 5° in Au(100). The chains have rotational freedom at room temperature, which means there is no three-dimensional order in the

arrangement of different chains. The adjacent chains are rotationally disordered and this persists at a low temperature. In fact, the freezing of the rotational disorder can be seen in low temperature infrared spectroscopy (Ref. 9). The presence of very bulky groups at the tail end can affect this order, as molecules may not get attached to all the available surface sites. The structure of alkane thiol monolayers on Au(111) is shown schematically in Fig. 5.3.

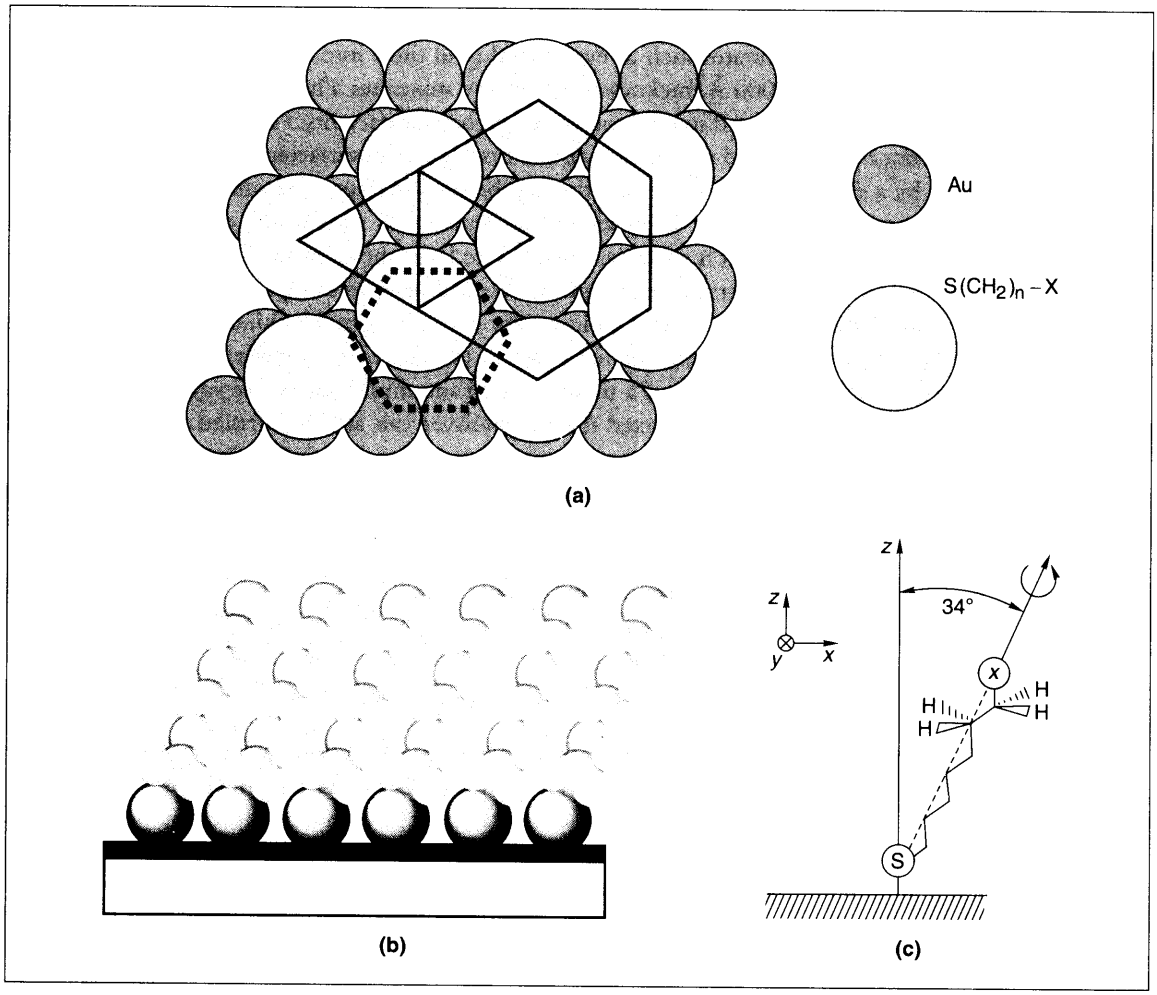

Fig. 5.3: *Schematic structure of a monolayer of alkanethiol on Au(111). (a) Layer of hexagonally arranged gold atoms (dotted hexagon). Each corner of this dotted hexagon corresponds to the center of the gold atom. On top of this surface, the alkanethiol molecules chemisorb. The structure of the sulphur atoms is also hexagonal (solid hexagon), as indicated. These atoms sit on three-fold sites created by the gold atoms. (b) Assembly of thiolate chains. This will form a two-dimensional sheet on the surface. (c) Extended chain. It shows a zig-zag assembly. The tilt angle is shown. It is also shown that the chains have rotational freedom. X is a functional group.*

As mentioned above, this structure is present for several hundreds of angstrom square area. The underlying surface itself is not ordered over an extended area and the typical grain size (within this region, the surface structure is uniform) is of the above dimension. This limits the growth of an ordered SAM over the entire area of the substrate. At the edges of the grain, the monolayer structure is not ordered due to defects in the structure of the gold. There are ways to increase the area of the ordered region such as high temperature annealing.

SAMs can be formed on other surfaces such as Cu, Ag, Pt, GaAs, etc. The coverage of molecules on these surfaces is in the order Cu>Ag>Pt>Au>GaAs, which is a direct consequence of the adsorbate structure. On Ag(111), the overlayer structure is the same as that of gold, but the tilt angle is only 12° and not 34°. This reduced tilt angle reduces the contact distance between the chains (4.1 Å and not 4.95 Å). On a GaAs(100) surface, a large tilt angle of 57° is reported (Ref. 10).

The chain length affects the order of the alkyl chain assembly. In the case of chains of longer thiols, the van der Waals interaction between the chains is large to enable all the chains to stand up. This makes the carbon chain assembly all-trans and reduces the number of defects. 'All-trans' means that the carbon atoms on either end of a C–C bond are trans to each other. This makes the alkyl chain appear like a zig-zag ladder-like structure. However, as the chain length decreases, the van der Waals interaction becomes weak and defects occur. These defects imply the incorporation of gauche conformations. The extent of order in the alkyl chain assembly manifested depends on the technique used for its investigation. The best tool to see the order is surface infrared spectroscopy, which shows a red shift in the methylene C–H stretches as a function of order. Peaks at 2918 and 2846 cm^{-1} are characteristic of ordered alkyl chain assembly. Decreased order is observed when the chain length is less than 11, and when the length is less than 6, the assembly is assumed to be disordered. When the groups at the chain ends have a smaller cross-sectional area than that of the alkyl chain (20 Å), the hydrocarbon chain assembly is the same as that of the alkyl thiol. This is the case with all monolayers with chain ends such as $-OH$, $-NH_2$, $-CONH_2$, $-CO_2H$, $-CO_2CH_3$ in addition to simple $-CH_3$. However, in the case of larger end groups, the chains cannot pack as efficiently as in the case of simple thiols.

The structure of the monolayer varies with the structure of the gold below it. Au(111) is thermodynamically the most stable surface due to the largest surface density of gold atoms. Therefore, in the case of evaporated or annealed gold, the surface is principally Au(111). A film of this kind can be grown on mica wherein the surface will be atomically flat. An atomic force microscopic image of octadecanethiolate monolayer grown on this Au(111) film is presented in Fig. 5.4. The image scale is 3.02 × 3.02 nm. The nearest neighbor is located at a distance of 0.52 × 0.03 nm (a) while the next nearest neighbor is located at a distance of 0.90 ± 0.04 nm (b) (Ref. 11).

Two binding modes of alkanethiol on a hollow site have been observed—one with the Au-S-C bond angle of 180° called the sp mode, and the other with Au-S-C bond angle 104° (sp^3 mode) (see Fig. 5.5). The energy difference between the two modes is 2.5 kcal mol^{-1}. Thus the thiolate can change from one mode to the other without much difficulty.

The overlayer structure of thiols on Ag(111) shows different types of lattice as shown in Fig. 5.6. The overlayer is of $(\sqrt{7} \times \sqrt{7})$ $R10.9°$ structure. The tilt angle in the case of thiols on Ag(111) surface is small as compared to gold. The observed value is about 5°. In some cases, the values were even close to zero

indicating that the chains are almost perpendicular to the surface. Also, the S-S distance in the case of SAMs on Ag(111) is close to 4.41 Å. Thus the van der Waals forces will be stronger in the case of silver.

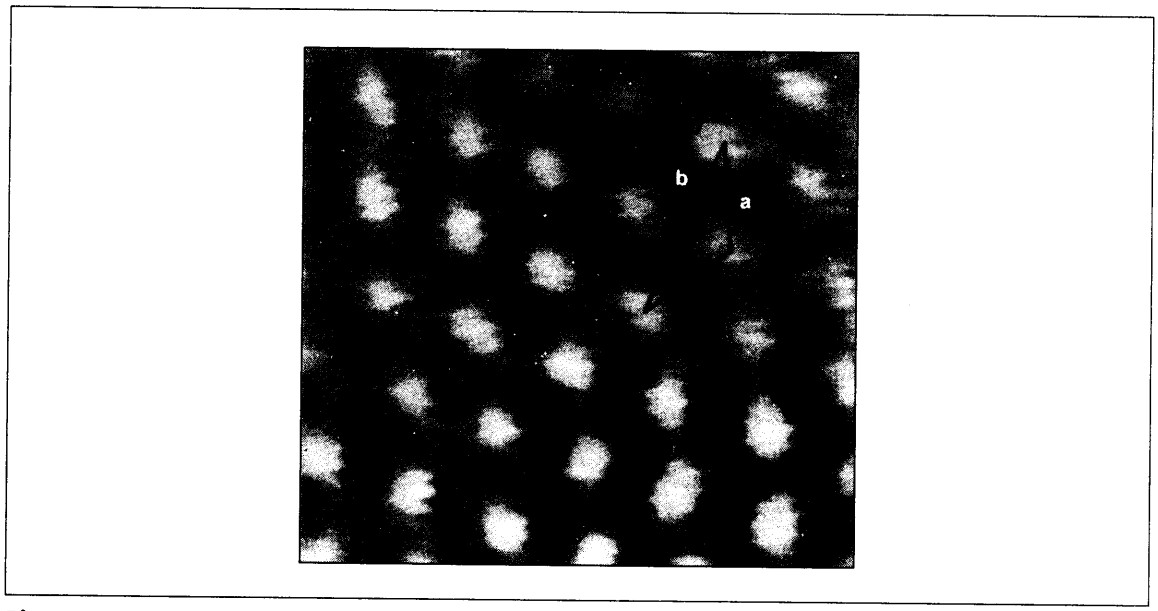

Fig. 5.4: *AFM image of octadecanethiolate on Au(111) (Ref. 11). Reprinted with permission from Alves, et al. (Ref. 11). Copyright (1992) American Chemical Society.*

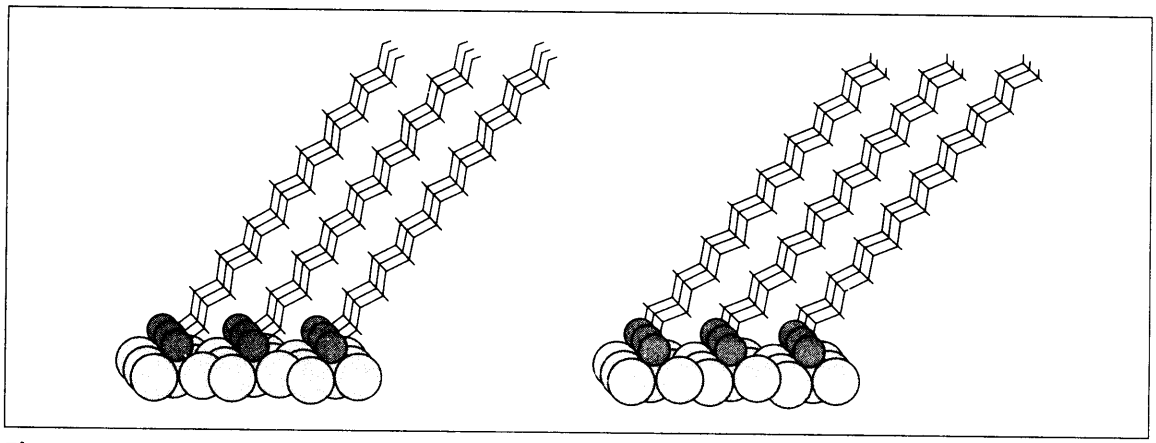

Fig. 5.5: *Nine molecule section of full coverage $C_{16}H_{33}SH$ monolayer on Au(111) based on molecular mechanics energy minimization calculation showing the tilted chains. Reprinted with permission from Ulman (Ref. 7). Copyright (1996) American Chemical Society.*

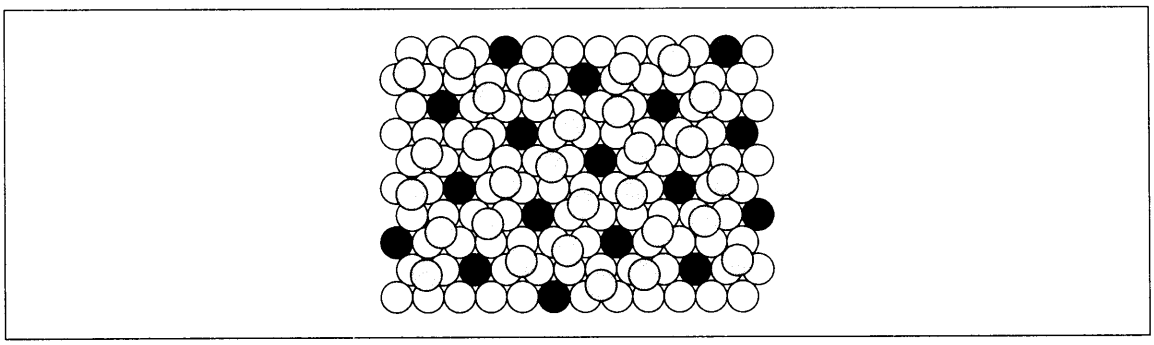

Fig. 5.6: *Overlayer structure of thiol on Ag(111). The open circles represent the silver atoms. The grey and black circles represent the sulphur at the hollow site and on-top site, respectively. Reprinted with permission from Ulman (Ref. 7). Copyright (1996) American Chemical Society.*

Another interesting result was observed in the case of the adsorption of fatty acids on metal oxide surfaces. The carboxylate group adsorbed symmetrically on the surface of silver oxide whereas in the case of aluminium oxide, the fatty acid molecules adsorbed asymmetrically with the tilt angle close to zero (see Fig. 5.7).

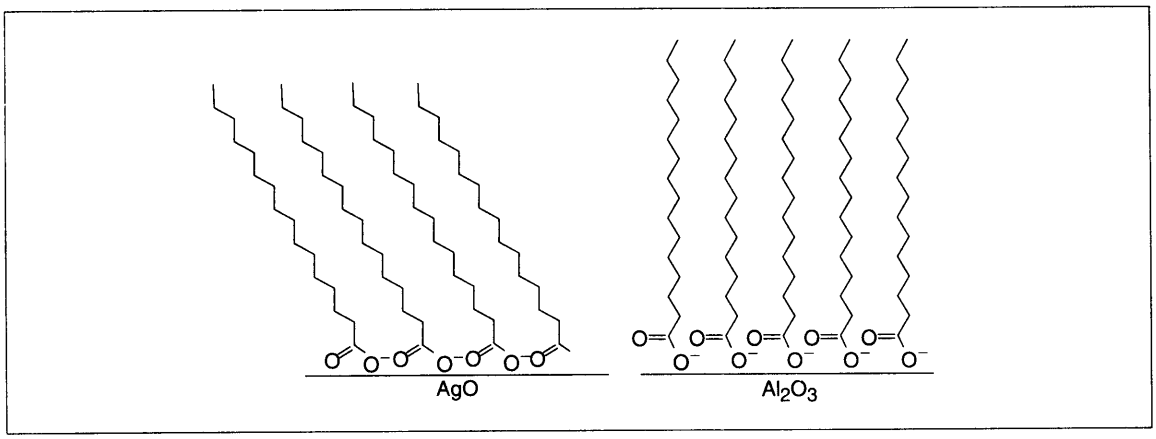

Fig. 5.7: *Orientation of alkyl chains on AgO and Al_2O_3 surfaces. In the case of AgO, the chains are tilted whereas in Al_2O_3, the chain is perpendicular to the surface. Reprinted with permission from Ulman (Ref. 7). Copyright (1996) American Chemical Society.*

The mechanism of thiol adsorption onto a gold surface is still not clear. One possibility is to treat it as an oxidative addition of R-S-H to the metal surface followed by the reductive elimination of the H_2 molecule from the metal surface. In an experiment, we have detected the evolution of hydrogen upon thiol chemisorption on gold surfaces.

$$R\text{-}S\text{-}H + Au_n \rightarrow R\text{-}S\text{-}Au^+ + Au_{n-1} + 1/2H_2$$

The energy of adsorption calculated from the RS-H (87 kcal mol^{-1}), H-H (104 kcal mol^{-1}) and the Au-SR bond energy (40 kcal mol^{-1}) taking the homolytic Au-SR bond strength is −5 kcal mol^{-1}. This value is in close agreement with the adsorption energy that Schlenoff calculated by using electrochemical data. This suggests that the value of 40 kcal mol^{-1} for the Au-S bond is probably correct.

Piezoelectric oscillators such as quartz crystal microbalance (QCM) can detect mass changes of the order of nanograms. This has been used to study the kinetics of monolayer adsorption. QCM is also used to detect the mass changes during the binding of monolayers with other molecules (for the basic principles of QCM, see Chapter 15).

Reflection-absorption infrared spectroscopy (RAIRS) can be used to derive useful information regarding the orientation of the alkyl chains on a metal surface. The spectrum is accumulated in the grazing reflection mode. In this mode, the incoming plane polarized laser light strikes the metal surface at a large angle of incidence. Only transition dipoles having a component perpendicular to the metal surface will be IR-active. If the chains are perpendicular to the metal surface, then $\nu_a(CH_2)$ and $\nu_s(CH_2)$ vibrations would be parallel to the plane of the surface and will be absent in RAIRS. In experiments, we see methylene vibrations indicating that the chains are tilted by a certain angle with respect to the normal surface.

The thickness of the monolayer is estimated by using ellipsometry. In this technique, a plane polarized laser light is used to probe the thickness. The plane polarized light reflected by a metal surface suffers both a phase change (Δ) as well as an amplitude change (Ψ). By comparing the covered and uncovered metal surfaces, one can find out the thickness as well as the refractive index of the monolayer. Porter, *et al.* (Ref. 11) studied a series of alkanethiols with n = 1, 3, 5, 7, 9, 11 and 21 to check the dependence of n (chain length) on the thickness of the monolayer. They found that for chains with $n \geq 7$, the measured thickness was less than the expected value. This indicates that the short chain members behave like a liquid with considerable disorder. Hence the values are less when compared to a chain in the all-trans configuration.

Angle dependent reflection of the P polarized light is used in surface plasmon resonance to study the thickness of the monolayer. At a certain angle of incidence called 'plasmon angle', laser light selectively excites the surface plasmon oscillations of the metal. This results in the absorption of light and a decrease in reflectance. The plasmon angle is very sensitive to the changes in the refractive index near the metal surface. This helps one detect the thickness of the monolayer on a metal surface.

It is essential to have an idea about the physisorption and chemisorption energetics for an understanding of the growth of the monolayer on a surface. The desorption of various thiols on Au(111) has been investigated by using specular helium scattering in combination with temperature-programmed desorption. In this technique, a helium beam reflected from the Au(111) plane is fed into a mass spectrometer tuned to m/z 4. A clean gold surface is able to reflect up to 30 per cent of the impinging helium beam. The adsorption of molecules onto the gold surface causes an increase in the diffuse scattering of the helium beam, consequently decreasing the specular intensity. When the molecules start desorbing, a greater part of the gold surface will be exposed to the helium beam, which increases the specular reflection. The

intensity of the specular signal will be maximum at the point of maximum desorption. The enthalpy of desorption can be calculated by using the Redhead equation from the value of temperature of maximum desorption (T_{des}) and heating rate, β, obtained from the temperature ramp experiment. From this, $E_{des} = R_g T_{des}[\ln(\nu T_{des}/\beta) - 3.64]$. R_g is the gas constant. ν is the pre-exponential factor in the Arrhenius expression. The typical value is 1×10^{13} S^{-1}. Two peaks were observed in the temperature-programmed desorption (TPD) of thiols on Au(111). The first peak occurring at a lower temperature in Fig. 5.8 is due to physisorption, while the second corresponds to chemisorption. The value for chemisorption was the same for most of the alkanethiols except for compounds wherein the steric effect can affect the bonding between the adsorbate and the substrate. Also the dialkyl sulphides do not show the chemisorption peak. This indicates that the dialkyl sulphides only physisorb on the surface. As the chain length increases, the van der Waals interaction increases and the contribution due to physisorption increases. For chains with n = 14, the two peak areas are comparable. For higher chain lengths, the van der Waals contribution becomes higher than that due to chemisorption. Since a long chain molecule is held on a surface by physisorption for a sufficiently long time, it has a greater chance of crossing the chemisorption energy barrier and thus of getting chemisorbed.

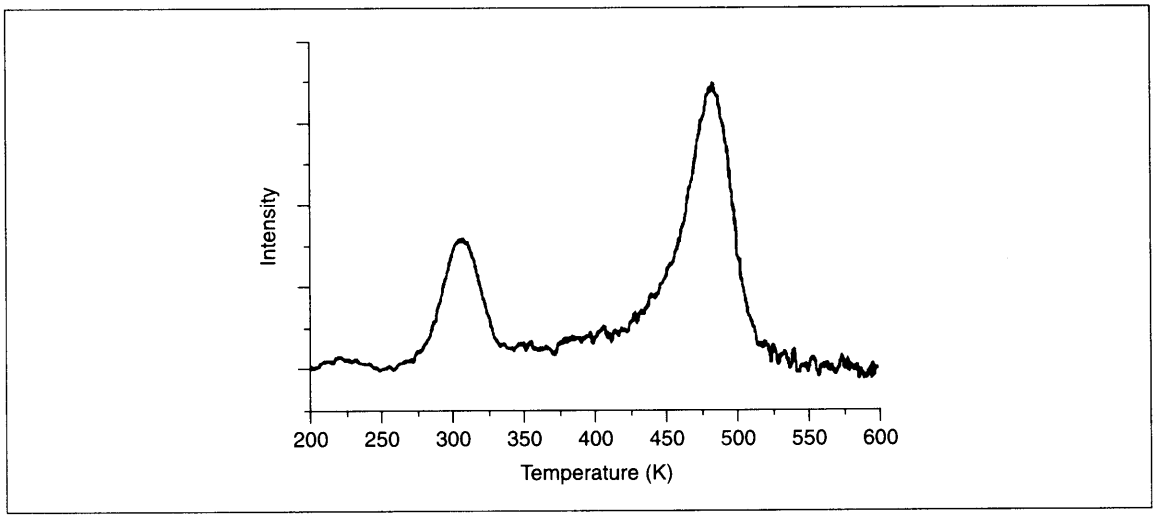

Fig. 5.8: *TPD spectrum derived from helium atom reflectivity signal as a function of temperature for hexanethiol on Au(111). Low temperature peak, which changes with the chain length, corresponds to physisorption and the high temperature peak, which is unaffected by the chain length variation, corresponds to the chemisorbed state. Reprinted with permission from Schreiber, et al. (Ref. 12). Copyright (1998) American Physical Society.*

In STM, the tunneling of the electron between the tip and the surface is used to image the surface. In AFM, the image is due to the force acting between the tip and the substrate. Both these techniques give atomic resolution. STM has been used to study the overlayer structure of adsorbates on metal surfaces (see Fig. 5.9).

In XPS, X-ray is used to knock out the core electrons. Deep core electrons do not participate in bonding. Their energies are characteristic of the atoms from which they originate. Hence XPS has been used to find the elemental composition of the monolayer. At lower take-off angles, the ejection of photoelectrons from the atoms at the top layer will be much more as compared to those from the deeper layers. Hence angle-dependent XPS can be used to find the composition of the monolayer.

The capacitive charging current in an inert electrolyte can be used to measure the thickness of the monolayer by the equation $C_{ML} = \varepsilon_0 \varepsilon_r / d$, where d is the thickness of the monolayer and C_{ML} is the capacitance of the electrode covered with a monolayer. ε_0 is the permittivity of the free space and ε_r is the dielectric constant of the separating material. By adding a redox couple, one can observe the Faradaic current. This gives the number of defects in the monolayer.

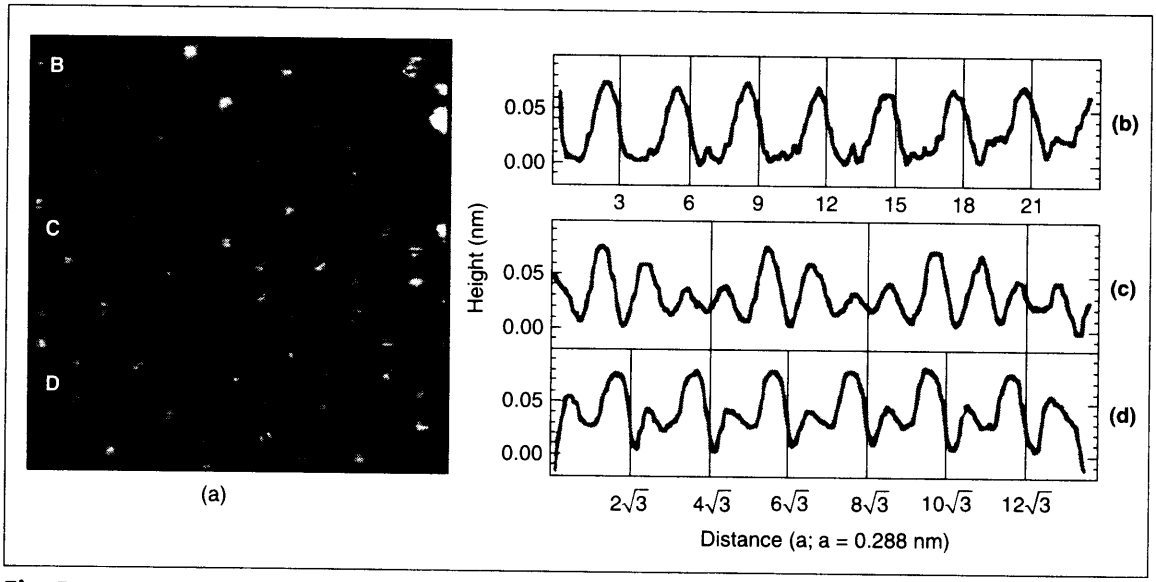

Fig. 5.9: *STM image of octanethiol on Au(111). Fig. 5.9(b) is the plot of the cross section labeled B in Fig. 5.9(a) running along the Au nearest neighbour direction. C and D are cross-sectional plots of Fig. 5.9(a) along the Au next-nearest-neighbour directions. Reprinted with permission from Poirier (Ref. 13). Copyright (1994) American Chemical Society.*

5.3 Growth Process

5.3.1 Growth from the Solution Phase

Various steps in the growth of monolayers are shown in Fig. 5.10.

The growth of the monolayer can be explained by using the Langmuir growth law. The rate of growth is proportional to the number of available sites given by the equation, $d\theta/dt = k(1 - \theta)$, where θ is the

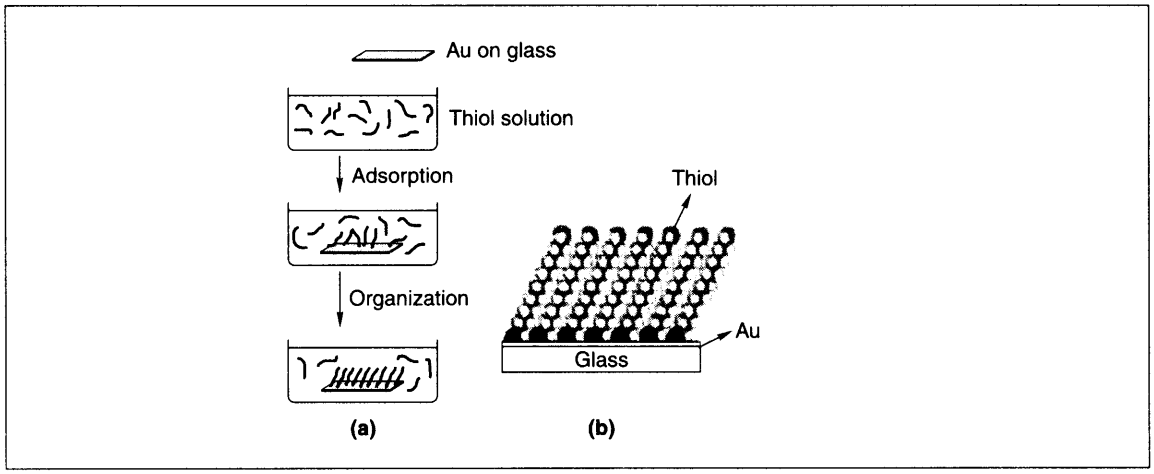

Fig. 5.10: *(a) Various steps during the formation of self-assembly. Gold coated glass slide is dipped in an ethanolic solution of thiol. The initial chemisorption process is very fast. This is followed by a slow step during which organization happens which takes several hours. (b) Structure of organized monolayer using a space filling model.*

fraction of sites occupied and k is the rate constant. Sum frequency generation (SFG) studies show three distinct steps during the growth of the monolayer. The first step corresponds to the chemisorption of the head group onto the metal surface and takes place very fast. Then the alkane chains start ordering into all-trans configuration, which is slower than the first process. During this straightening of the alkyl chain, the signal due to the d_- mode (antisymmetric CH_2 vibration) decreases in intensity. The gradual reorientation of the terminal methyl group during the final step is indicated by the slow evolution of r^+ mode (symmetric CH_3). The evolution of different modes is shown in Fig. 5.11.

5.3.2 Growth from the Gas Phase

The growth of monolayer from the gas phase in UHV allows one to study the process by using various *in-situ* measurements. The study by low energy electron diffraction (LEED) shows that the first phase, occurring immediately after dosing with the adsorbent molecule, is the stripped phase. On continued deposition, the structure changes to the standing phase with C (4×2) lattice.

The growth of mercaptohexanol monolayer on a gold surface has been investigated by using STM (see Fig. 5.12). Exposing the surface to low concentration of mercaptohexanol gives strips as shown in Fig. 5.12 (pointing finger, Fig. 5.12(b)). In these strips, the sulphur atoms will be sitting in the next-nearest-neighbour three-fold hollow sites and the alkane chain will be parallel to the substrate. On increasing the dosing, this stripe starts growing and covers the whole surface (Fig. 5.12(c) and Fig. 5.12(d)). Towards the end of saturation, a new feature called 'islands' starts appearing (pointing finger, Fig. 5.12(e)). From this point onwards, the growth starts taking place in the perpendicular direction and the alkane chain will be

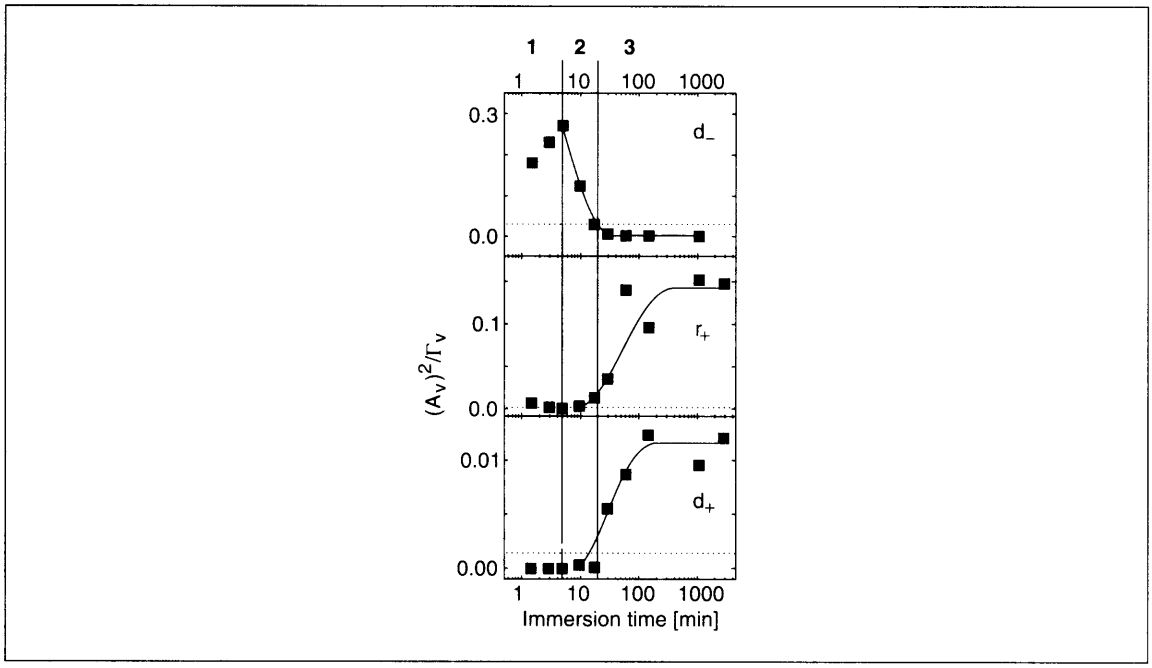

Fig. 5.11: *Intensities of the various modes upon the a adsorption of docosanethiol on Au(111). The three regions indicate the three steps during the growth process. Intensity of the features is plotted as a function of immersion time. Reprinted with permission from Schreiber F. (Ref. 14). Copyright (2000), with permission from Elsevier.*

perpendicular to the substrate in these islands. The Au vacancies will appear as deep pits after the island formation (Fig. 5.12(f)).

Even though the stripped phase with the alkane chain parallel to the surface, and the standing up phase with the alkane chain perpendicular to the surface, are the two important phases during the growth of the monolayer, metastable phases exist between the two extremes. This has been shown in Fig. 5.13.

5.3.3 Stability and Surface Dynamics

The thermal stability of SAMs depends on: (1) the strength of surface binding, and (2) the strength of lateral interaction. For alkanethiols on gold the thermal stability increases as a function of the chain length. While butanethiol monolayers desorb starting from a temperature of 75 °C, octadecane monolayers desorb at temperatures ranging from 170 to 230 °C (Ref. 15). Increasing the lateral π–π interaction increases the thermal stability. Electrochemically the stability range of −0.1 to +0.1 V is very high, providing a large electrochemical window for most applications. This implies that a number of electrochemical processes can be conducted without monolayer desorption. The exposure of shorter chain thiols in solution can

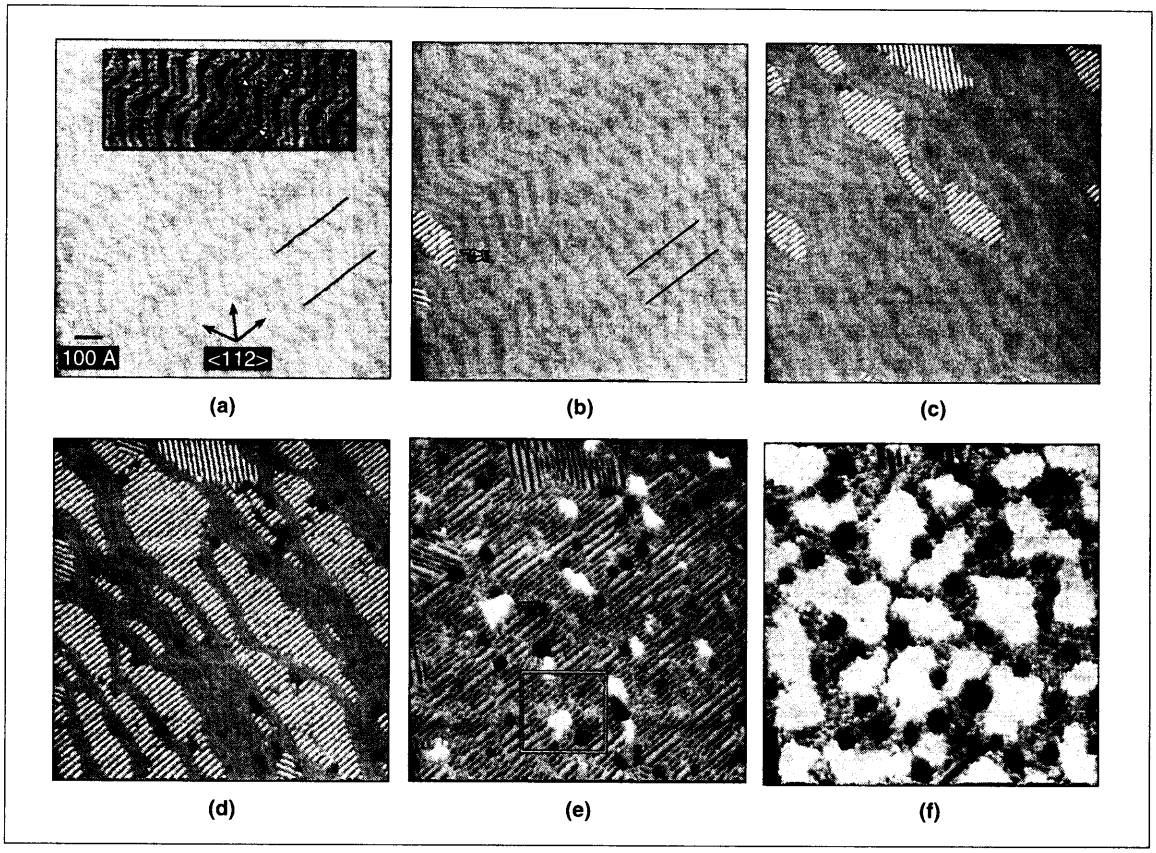

Fig. 5.12: *Constant current STM topographs showing the growth of mercaptohexanol monolayer from gas phase on Au (111) surface. (a) Clean Au (111) surface. (b) Stripped phase islands. (c) Striped phase growth. (d) Stripped phase growth showing Au vacancies. (e) Growth of standing up phase at the cost of the stripped phase. (f) Standing up phase growth at saturation limit. Reprinted with permission from Schreiber F. (Ref. 14). Copyright (2000) with permission from Elsevier.*

lead to the removal of defects on the SAM surface. This occurs by the exchange of monolayers at the grain boundaries, called 'ligand place exchange' and the diffusion of the monolayers, which occurs over a time window of several hours. The exposure of reactive gases such as ozone can affect the stability of the monolayer as the thiolate group can be oxidized (Ref. 16).

5.4 Phase Transitions

As a result of the van der Waals interaction, alkane thiol monolayers form crystalline phases on the metal surface. But as the temperature of the system increases, the orientational disorder increases. This weakens

of the molecules. In this approach, the ink can be made of a variety of materials including nanoparticles. The approach need not necessarily make a monolayer.

If the substrate can be controlled in such a way that deposition occurs only in the selected areas, patterns can be drawn. In one such approach, the potential was controlled on an array of electrodes. If this is done on selected areas of an already coated electrode, a part of the monolayers can be desorbed and another monolayer can be coated on such locations. It is also possible to control the potential on specific areas of an uncoated electrode to accelerate or decelerate deposition. Both these approaches have been used to make patterned monolayers.

5.6 Mixed Monolayers

One can obtain a mixed monolayer by mixing two monolayer forming species in an appropriate ratio. If the chemical constitutions of the two monolayer-forming entities are similar in terms of the alkyl chain length and the functionality, the mixed monolayer is similar to a two-dimensional alloy (two-dimensional in the sense that the film is planar, while the thickness is molecular). However, chemical differences between the species can lead to the segregation of one entity. If the two chemical constituents are separated, it is possible to anchor two different kinds of materials at these locations by using selective molecular chemistry.

5.7 SAMS and Applications

5.7.1 Sensors

The interest generated by the study of SAMs has shifted from fundamental studies to technology. The potential applications of SAMs include molecular recognition and wetting control. The chemical properties of the monolayers can be used for sensing applications. There are two important elements in a sensor, of which the first is the chemically selective recognition layer, while the second is the signal transducer which provides a signal that can be monitored. A number of approaches have been used to make selective recognition layers, which depends on the species to be detected. The fact that several of these sensing elements can be located on a given area provides the capability to sense several species simultaneously (see Chapter 12).

A variety of metal ion sensors can be made by functionalizing the metal surface with a ligand with high specificity to a particular ion. Sensors selective to Cu^{2+} were made by functionalizing the gold surface with 2,2′-thiobisethyl acetoacetate. The selective detection of perchloroethylene in the presence of other molecules such as trichloroethylene, tetrachloromethane, chloroform, and toluene was achieved by using modified resorcin(4)arene as the monolayer (see Fig. 5.14). The incorporation of perchloroethlelene

into the receptor site results in mass changes in terms of nanograms, which are detected with the help of a quartz microbalance oscillator.

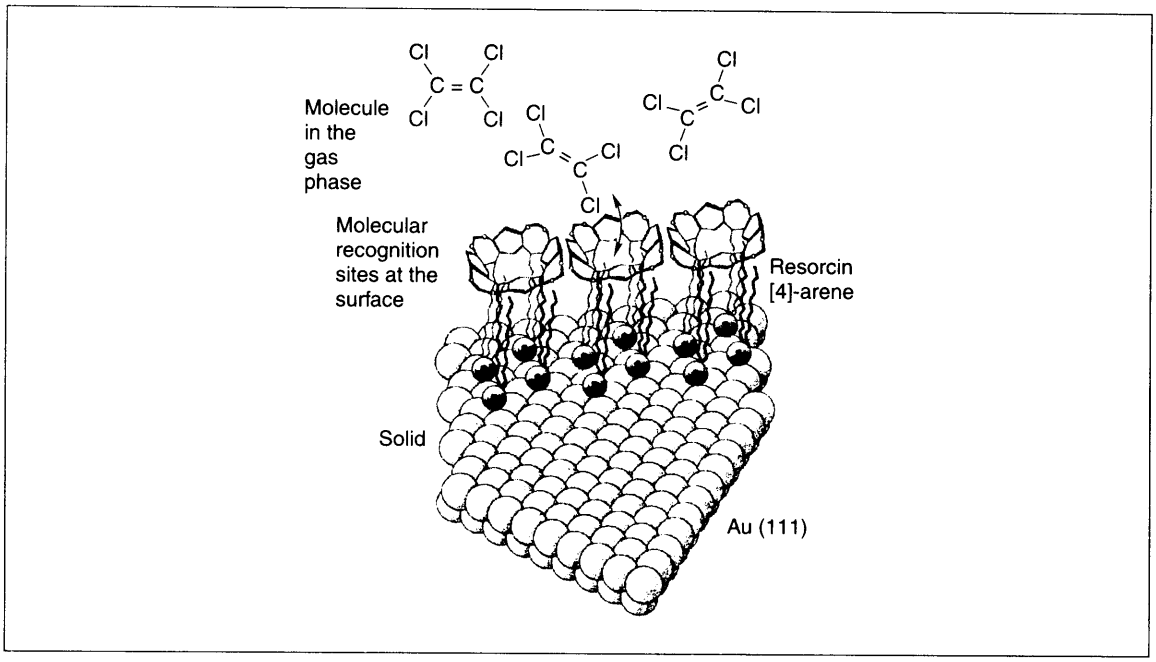

Fig. 5.14: *Molecular recognition by a monolayer of resorcinol on Au (111) surface. The receptor site showed high selectivity to perchloroethylene when dosed with a mixture of halocarbons. Reprinted with permission from Schierbaum, et al. (Ref. 24). Copyright (1994) AAAS.*

Among the most common examples of SAM-based sensors are enzyme biosensors. As enzymes are catalytic in action, they are also called catalytic biosensors. Here an enzyme acts as the recognition element. The signal is transduced by detecting either the molecule consumed or that generated. An example of this kind of sensor is the glucose biosensor which uses glucose oxidase (GOD), to oxidize glucose to gluconolactone. In this process, the enzyme is reduced and a mediator used in the process gets the enzyme back to the original state. In nature, O_2 is the oxidizer and H_2O_2 is produced in the process. The mediators used typically in experiments are ferrocene and ferricyanide, and their change is monitored electrochemically. The reduced form of the mediator gets oxidized at the electrochemical surface and the current generated is proportional to the amount of glucose oxidized. The immobilization of the enzyme is more controlled when it takes place on a SAM surface.

Enzyme immobilization on the monolayer surface can be achieved by several means. One method is to covalently modify the SAM by selected reactions. An approach used for this is described below. Here a mercaptopropionic acid monolayer is made on Au. The monolayer is activated by reacting with 1-ethyl-3(3-dimethylaminopropyl)carbodiimide hydrochloride (EDC) and N-hydroxysuccinamide (NHS). This process makes a succinamide ester on the monolayer surface, helping amine groups of the enzyme to

bind to the surface, thereby forming an amide linkage. There are other approaches such as the use of electrostatic interactions. The approach mentioned here is illustrated in Fig. 5.15. An excellent review is available on the preparation of sensors on monolayers (Ref. 25).

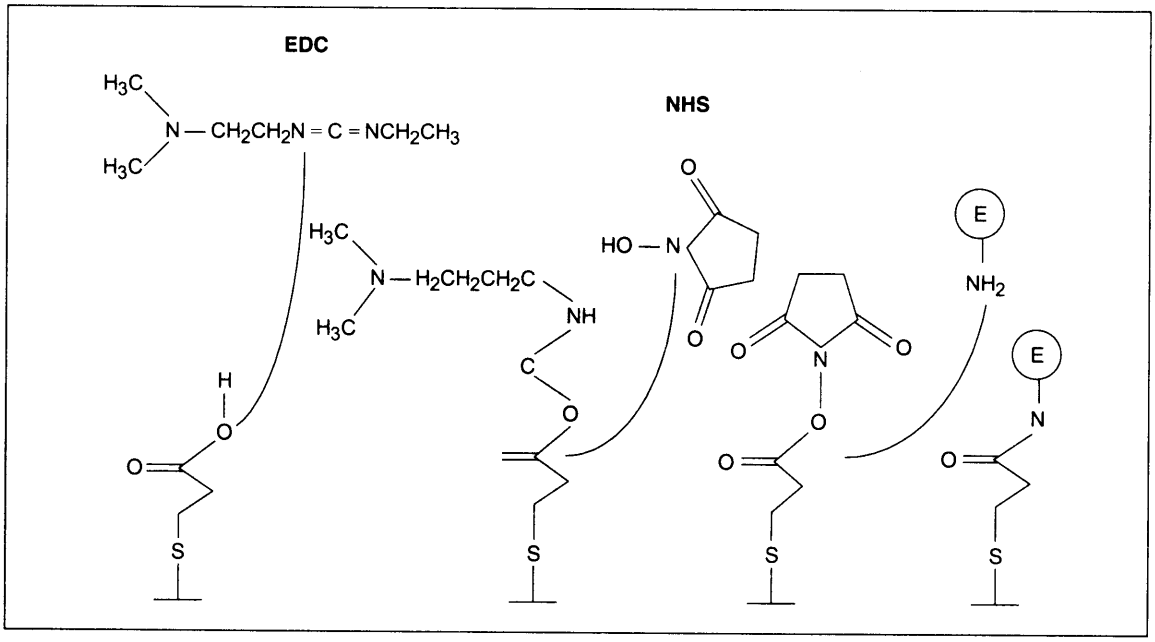

Fig. 5.15: *An approach used to achieve enzyme immobilization. E is an enzyme.*

5.7.2 Affinity Biosensors

In these sensors, a biorecognition molecule is the sensor element, which is specific to the analyte molecule. Depending on the sensor molecule, which can be in the form of antibodies, proteins, DNAs, etc. various analyte species can be detected. The recognition event needs to be sensed. The most common approaches for sensing are surface plasmon resonance and quartz crystal microbalance (QCM). In the former, the change in the surface plasmon resonance of a thin film of gold as a result of the biorecognition event is used to sense the event. In the QCM method, the change in the oscillation frequency of a quartz crystal as a result of the mass accumulation on a gold film deposited on its surface, is used to sense the biorecognition event.

The biorecognition molecule must be immobilized on the surface. One protocol used for this purpose is to thiolate the biomolecule. In the case of a DNA the 5′ end can be thiolated by a mercaptohexyl unit and a solution of the DNA upon exposure to the gold surface forms a monolayer. However, the single-stranded DNA (ssDNA) lies on the gold surface and as a result, the hybridization efficiency is reduced to 10 per cent. By exposing the thiolated DNA surface to mercaptohexane (MCH), the locations wherein

the DNA is not pinned, are occupied by the monolayer, which makes the DNA stand up. This facilitates specific binding and the hybridization efficiency is enhanced to 100 per cent (Ref. 26).

The immobilization of biomolecules can be used for various applications. By immobilizing an antibody specific to a bacterial strain, the sensor can detect that specific bacterium. This has been demonstrated (Ref. 27) for *salmonella paratyphi* with specificity to other serogroups of *salmonella* and the detection limit found was 1.7×10^2 cells/mL. Various kinds of species can be detected on the basis of the immobilized biomolecule.

An affinity biosensor can behave like a nanomachine. This has been demonstrated with an ion channel biosensor. Here a gramicidin ion channel has been used as a sensor and the transduction is achieved by measuring the conductivity (Ref. 28). Gramicidin is an example of a channel found in cell walls. It is an unusual peptide, having alternating D and L amino acids. In lipid bilayer membranes, as in the case of a cell wall, gramicidin dimerizes and folds as a right handed β helix. The dimer just spans the bilayer. In the mechanism of ion transport through membranes, it has been found that the ion transport rate depends on gramicidin because the gramicidin channel functions when the proteins reversibly dimerize on the membrane, thereby opening up a channel. This is illustrated in Fig. 5.16.

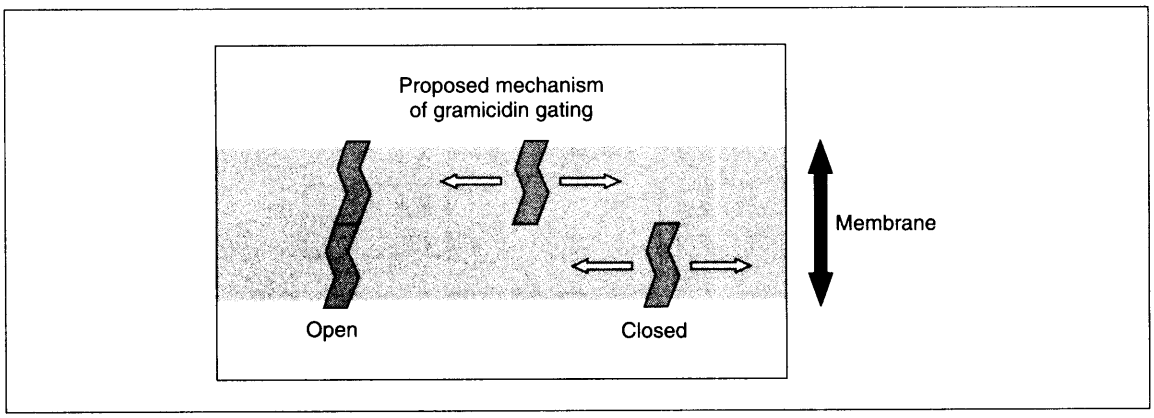

Fig. 5.16: *Mechanism of opening and closing of ion channels by gramicidin. Gramicidin (shaded) moves on the membrane and locking of two units opens the ion channel.*

In the sensor, the gramicidin (IG) is thiolated and immobilized on the surface. It is separated with thiols which act as spacers (ST). A lipid bilayer is anchored onto the SAM through tethered lipids (TL), which penetrate into the lower half of the bilayer. The upper half of the bilayer has mobile gramicidines (MG) with pendent biotin groups. Membrane spanning lipids (MSL) are also anchored to biotin groups. Antibody fragments (Fab) are linked to MG and MSL units through streptavidin (S) using biotin. In the open state, the MG units are mobile and as a result, MG and IG get linked, thereby opening up the ion channel. This leads to a large increase in conductivity. When analyte molecules (A) are present, MG cannot diffuse freely, as these molecules are locked in position. Depending on the antibody fragments used, this sensor can work for different analytes. Its use has been demonstrated in the case of hormones, bacteria and certain sequences of DNA (Ref. 29). The working principle of the sensor is illustrated in Fig. 5.17.

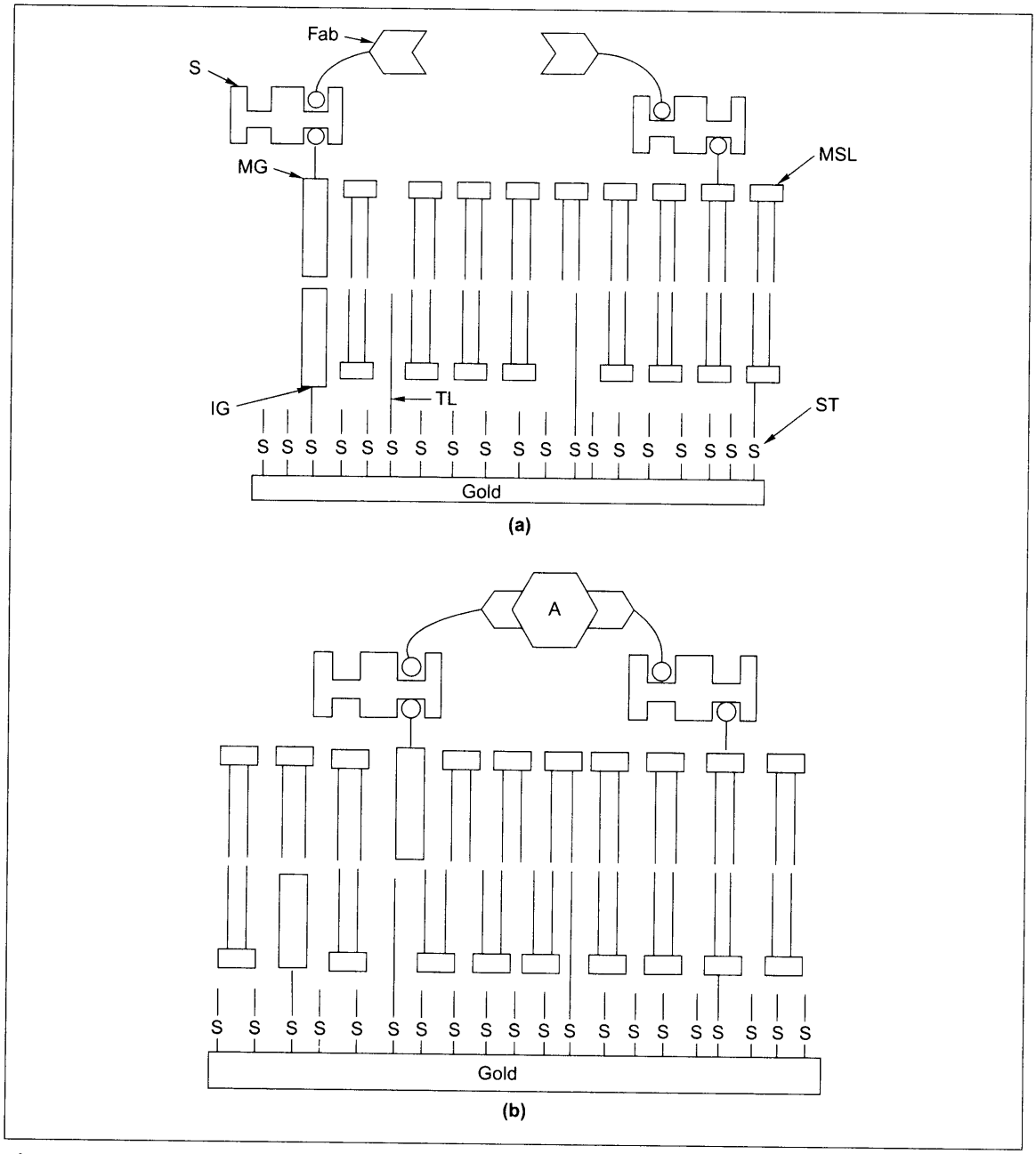

Fig. 5.17: *Schematic illustration of the ion channel based bio sensor (Ref. 28). When MG and IG coincide, a large increase in ionic conductivity is observed as gramicidin ion channel opens up (a). When the analyte blocks the antibody fragments, the movement of gramacidins become impossible, reducing the ionic conductivity (b). Adapted from Ref. 28. Copyright Nature.*